HORIZONTAL STRAIN RATES OF THE JAPANESE ISLANDS ESTIMATED FROM QUATERNARY FAULT DATA

Sohei KAIZUKA and Toshifumi IMAIZUMI

Abstract Average rates of horizontal strain during the Quaternary in the Japanese Islands are calculated from active fault data. Although the directions of the maximum compressive strains are in harmony with those obtained from seismological and triangulation data, the magnitude of the strain rates of shortening (mainly $10^{-9}\sim10^{-8}$/yr) is much smaller than that obtained from triangulation data (mainly $1\sim2\times10^{-7}$/yr). An important factor in causing this difference may be non-elastic shortening of the crust under compressional stresses.

1. Introduction

Data of uniform quality on all Quaternary active faults in Japan were presented in 1980 in the book entitled 'Active Faults in Japan: sheet maps and inventories' by the Research Group for Active Faults (RGAF, 1980a), and a summary article of that book was also written by the Research Group (RGAF, 1980b). Based on the data on Quaternary active faults in the book, we calculated the average rates of horizontal shortening and extension and their strain rates for the Japanese main islands and the borderland off the Japan Sea coasts of Hokkaido and Honshu. The area covers the intraplate zone of the Japanese island are exclusive of the subduction zone off the Pacific coasts of the Japanese main islands.

The procedure of the calculation is described in chapter 2, and the results obtained are shown in chapter 3; in chapter 4 the results are discussed and compared with horizontal strain rates obtained from seismological and geodetical data and from Quaternary folds. In this introduction we give a short explanation of the book on active faults (RGAF, 1980a), as the main source of basic data for this article.

In the book, all Quaternary active faults on land, recognized by the interpretation of aerial photographs supplemented by geological maps and field surveys, are mapped at 1:200,000 and listed. Each fault is classified into one of three categories in terms of certainty: (I) certain beyond doubt that the fault was active during the Quaternary; (II) though not definitely certain, it is possible to infer the sense of the displacement; (III) the fault is a mere lineament suspected to be active during the Quaternary. For every land fault in categories I and II, the following fault parameters are listed as much as possible: degree of fault activity, fault length, strike, dip, fault trace feature, fault reference, age of fault reference, fault displacement, average slip rate, and references. The degree of fault

activity is classified as A. B, or C, on the basis of the average rate given by the amount of displacement over time of a reference surface or a line: (A) for 10 – 1 m/1000 yr, (B) for 1 – 0.1 m/1000 yr, and (C) for 0.1 – 0.01 m/1000 yr.

Submarine active faults beneath the sea around the main islands of Japan, which were recognized by the use of seismic reflection profiles, are mapped at 1:2,000,000. On this map, submarine active faults are classified by height of fault scarp: more than 200 m and less than 200 m.

Figure 1 represents the distribution of the active faults on land and beneath the sea based on the book of active fault (the 4th printing (1981) of RGAF, 1980a). In this map, all active faults on land in certainty categories I and II are shown in terms of their activity (A, B, C, and unknown), and in terms of their fault type (dip-slip, right-lateral strike-slip, and left-lateral strike-slip). Nearly all dip-slip faults in Figure 1 are thought to be thrust faults except for some normal faults in central Kyushu (RGAF, 1980a; see Table 1).

The relation between the Quaternary active faults given by the book and destructive earthquakes and earthquake faults, which occurred during the historical age, was studied by Matsuda (1981) and Kakimi (1983), and a mutual relationship in spatial distribution was found.

The outline of this article was read at the annual meeting of the Seismological Society of Japan in 1981 (Kaizuka and Imaizumi, 1981).

2. Method of Calculation of Strain Rates from the Quaternary Active Faults

Directions of horizontal maximum shortening and setting of grids for the calculation of strain rates

The directions of horizontal maximum shortening deduced from strikes and the type of Quaternary active faults on land are represented in Figure 2 (a). They are in harmony with trajectories of the horizontal maximum compressional stress directions shown in Figure 2 (b), which were deduced from various sources, i.e., dikes of Quaternary volcanoes, mechanisms of earthquakes, and in-situ rock-stress measurements. Moreover, the directions of maximum shortening deduced from the changes in horizontal angles of the first-order triangulations (Fig. 11) show nearly the same pattern as that obtained from the active faults. These facts indicate that the Quaternary active faults have been formed under stress conditions similar to the present tectonic stress fields in Japan.

In order to calculate the rates of horizontal shortening and extension caused by active faults and their strain rates, the large and small grids, whose sizes are 80×80 km^2 and 40×40 km^2, were closely set without remarkable overlaps (small grids are used for the areas where faults are dense and axes of maximum shortening are changing direction). At that time, the boundaries of active fault provinces (Fig. 3 and Table 1, after RGAF, 1980b) were taken into consideration, and at the same time, the upper and lower sides of a grid were set parallel to the direction of the horizontal maximum shortening of the area (Fig. 4). Grid numbers were assigned to each active fault province.

In the region off the Pacific coast of Japan, where the Pacific and Philippine Sea plates have been subducted under the Eurasia plate, because of the lack of sufficient data with

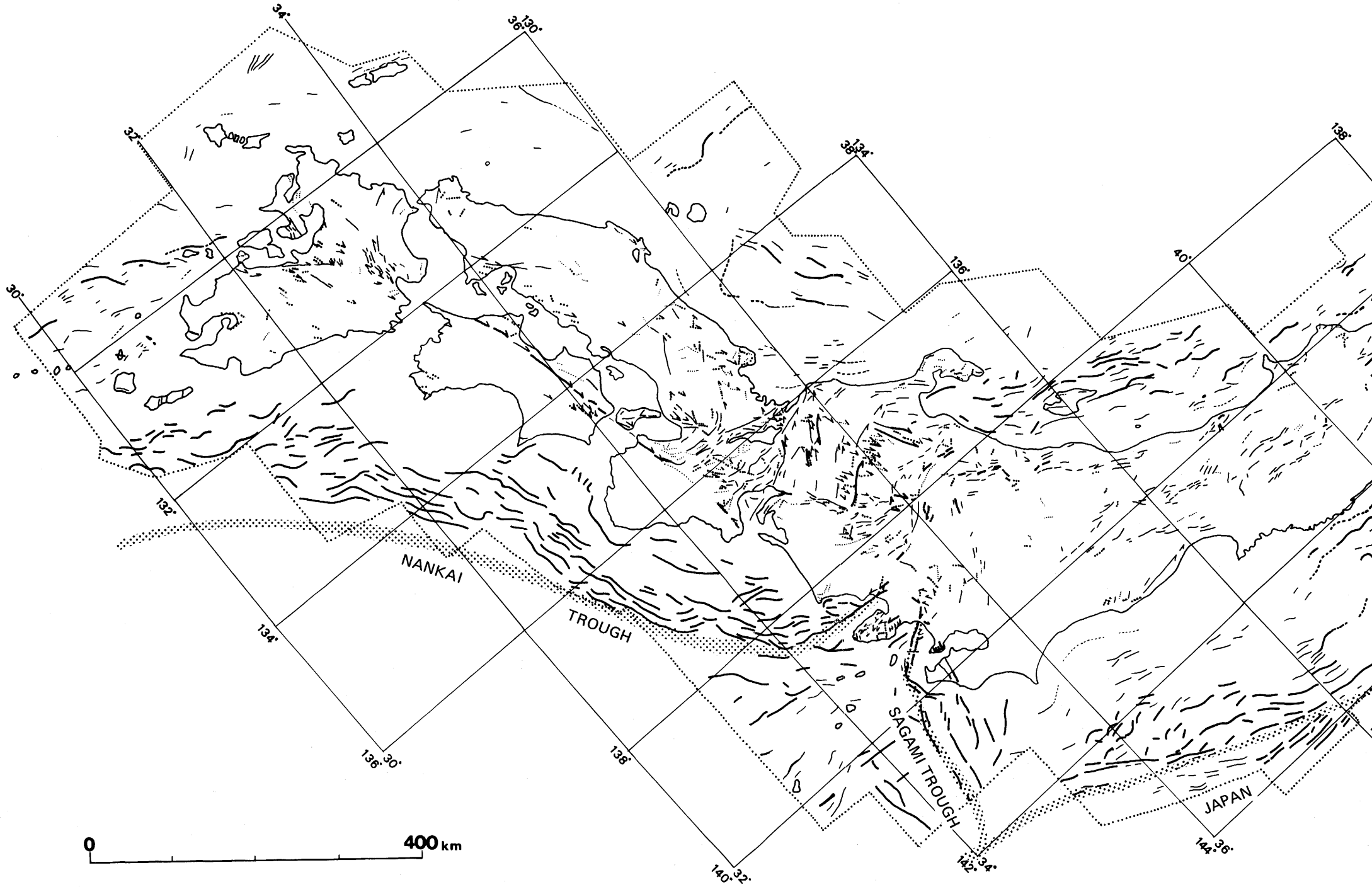

Fig. 1 Quaternary active faults in and around Japan (after the 4th printing (in 1981) of RGAF, 1980a).

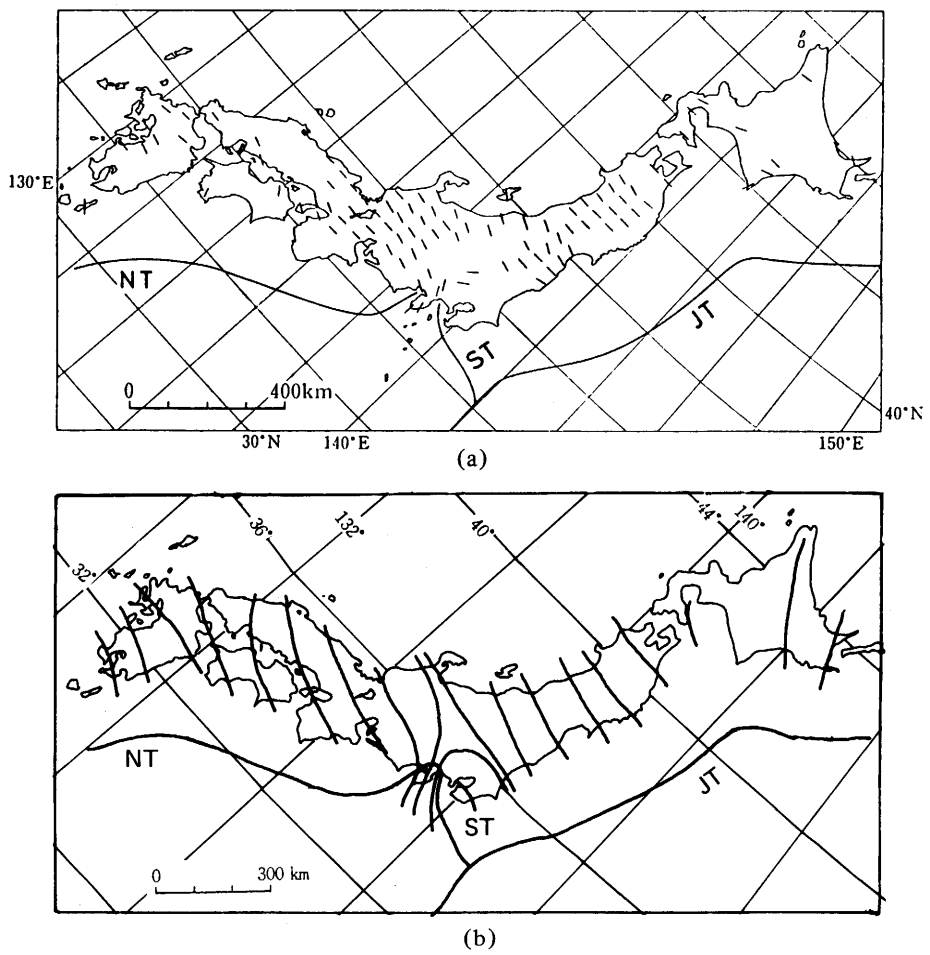

Fig. 2 (a) Directions of the horizontal maximum shortening deduced from Quaternary active faults on land (RGAF, 1980a).
(b) Trajectories of the horizontal maximum compressional stress directions deduced from various sources: Quaternary active faults, dikes of Quaternary volcanoes, mechanisms of earthquakes, and in-situ rock-stress measurements (Matsuda et al., 1978).
JT: Japan Trench, NT: Nankai Trough, ST: Sagami Trough.

regard to the slip rates of many faults, calculation of horizontal strain rates in that subduction zone was excluded from this study.

Calculation of horizontal strain rates

The procedure of calculating horizontal strain rates in each grid is shown in Figure 5. Separate calculations are made for two fault types: dip-slip type and strike-slip type.

Dip-slip type (case I in Fig. 5)

First we measured the total length of each class fault (la, lb, lc) in a grid (Figs. 5-(1) and

Table 1 Characteristics of active fault provinces in Japan (RGAF, 1980b)

Province	Sub-province	Density of faults	Length of major faults	Activity of major faults	Types of faults	Note
I. Main part of Hokkaido	a. inner belt of main Hokkaido	low	short	C	reverse?	
	b. outer belt of main Hokkaido	low	medium	B	reverse	
II. Inner belt of NE Japan	a. continental slopes of inner belt of NE Japan	high	long	A?	reverse	sea-bottom
	b. inland of inner belt of NE Japan	medium	short	B	reverse	volcanic region
III. Outer belt of NE Japan		very low	medium	B	reverse·strike-slip?	
IV. Continental slopes off the Pacific coast of NE Japan	a. off the south coast of Hokkaido	high	long	A?	reverse·strike-slip?	sea-bottom
	b. off Sanriku-Joban-Kashima	high	long	A?	reverse	sea-bottom
	c. around Sagami Trough	high	long	A	reverse·strike-slip	mainly sea-bottom
V. Northern tip of Izu-Ogasawara arc	a. around the Kanto Mountains	medium	short	B	reverse·strike-slip	
	b. around Izu Peninsula	high	short	B	strike-slip	volcanic region
BF. Western Fossa Magna belt		high	short	A	strike-slip·reverse	
VI. Eastern part of inner belt of SW Japan	a. around Noto Peninsula	low	short	B.C	reverse	land & sea-bottom
	b. around Oki Trough	medium	medium	B?	reverse?	sea-bottom
	c. Chubu Mountains	high	long	A	strike-slip·reverse	
	BT. Tsuruga Bay-Ise Bay Line belt	high	medium	A.B	strike-slip·reverse	
	d. Kinki triangle	high	medium	B.A	strike-slip·reverse	
	e. northwestern part of Kinki district	medium	medium	B	strike-slip·reverse	
VII. Western part of inner belt of SW Japan	a. Chugoku-Setouchi-northern Kyushu	low	short	B.C	strike-slip·reverse	
	b. volcanic field of central Kyushu	high	short	B	normal	volcanic region
BM. Median Tectonic Line belt		high	long	A	strike-slip	
VIII. Outer belt of SW Japan		very low	short	B.C	reverse·strike-slip	
IX. Continental slopes off the Pacific coast of SW Japan		high	long	AA	reverse·strike-slip	sea-bottom
X. Northern part of Okinawa Trough		medium	long	B?		sea-bottom
Nansei Islands		high-low	short	B.C	normal	land only
Izu-Ogasawara Islands		low?	short	C	reverse?	land only

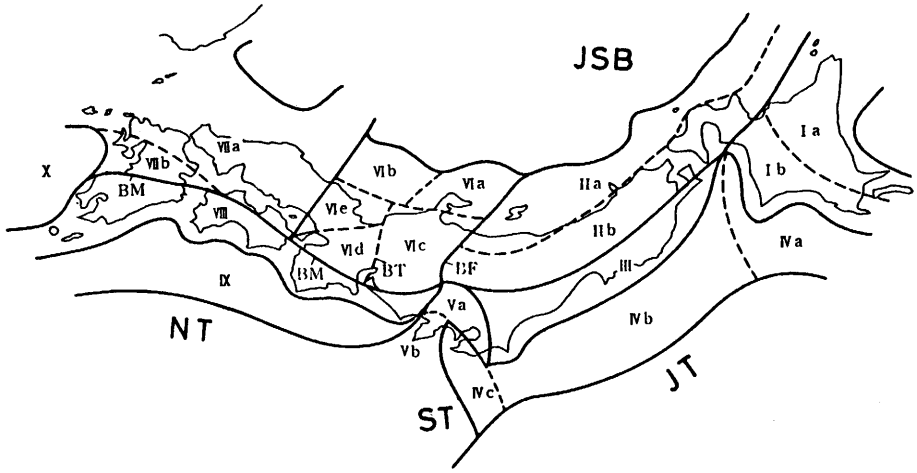

Fig. 3 Active fault provinces of Japan.
JT: Japan Trench, ST: Sagami Trough, NT: Nankai Trough, JSB: Japan Sea Basin. (cf. Table 1 for the nature of respective provinces). (RGAF, 1980a)

(2)). At this time, strikes of all dip-slip faults in a grid (except normal faults in the province VIIb) were considered to be perpendicular to the direction of shortening – that is, in practice, perpendicular to the upper and lower sides of the grid concerned – although some faults are oblique to the direction of shortening within 30 degrees.

Next the total length of each class fault was transfered to the number of the normalized A class fault (N_A), the length of which is the same as the length of a side of the grid concerned (Fig. 5-(3)). The faults whose activity is unknown were regarded as class B faults. The number of class-unknown faults on land is about 10 percent of the total number of active faults in certainty categories I and II. Submarine faults with scarp heights greater than 200 m and less than 200 m were regarded as class B and class C faults, respectively.

Then we calculated the rate of shortening (R^-) or extension (R^+) per year on the assumption that the dip angle of every fault plane is 45 degrees (Fig. 5-(4)). This assumption seems to be supported by the fact that dip angles of reverse faults in Japan, exclusive of large thrust faults in the subduction zone off the Pacific coast, are mostly within 45±15 degrees, according to the data on the mechanisms of shallow large earthquakes (*e.g.*, Usami, 1975; Wesnousky *et al.*, 1982). Under this assumption, it is evident that the vertical displacement or vertical strain rate of a thrust fault is immediately equal to the horizontal displacement or horizontal strain rate of shortening. The dip angle of every normal fault is also assumed to be 45 degrees. In the area in Figure 1, known active normal fault are few and short in length; the distribution is restricted mostly to central Kyushu (active fault province VIIb, cf. Table 1).

Finally, we divided the rates of shortening or extension by the space of the grid concerned (Fig. 5-(5)), and got the strain rates of shortening (ϵ^-) or extension (ϵ^+), respectively.

Strike-slip type (case II in Fig. 5)

The total length of each class of fault (L_A, L_B, L_C) was measured. This length was trans-

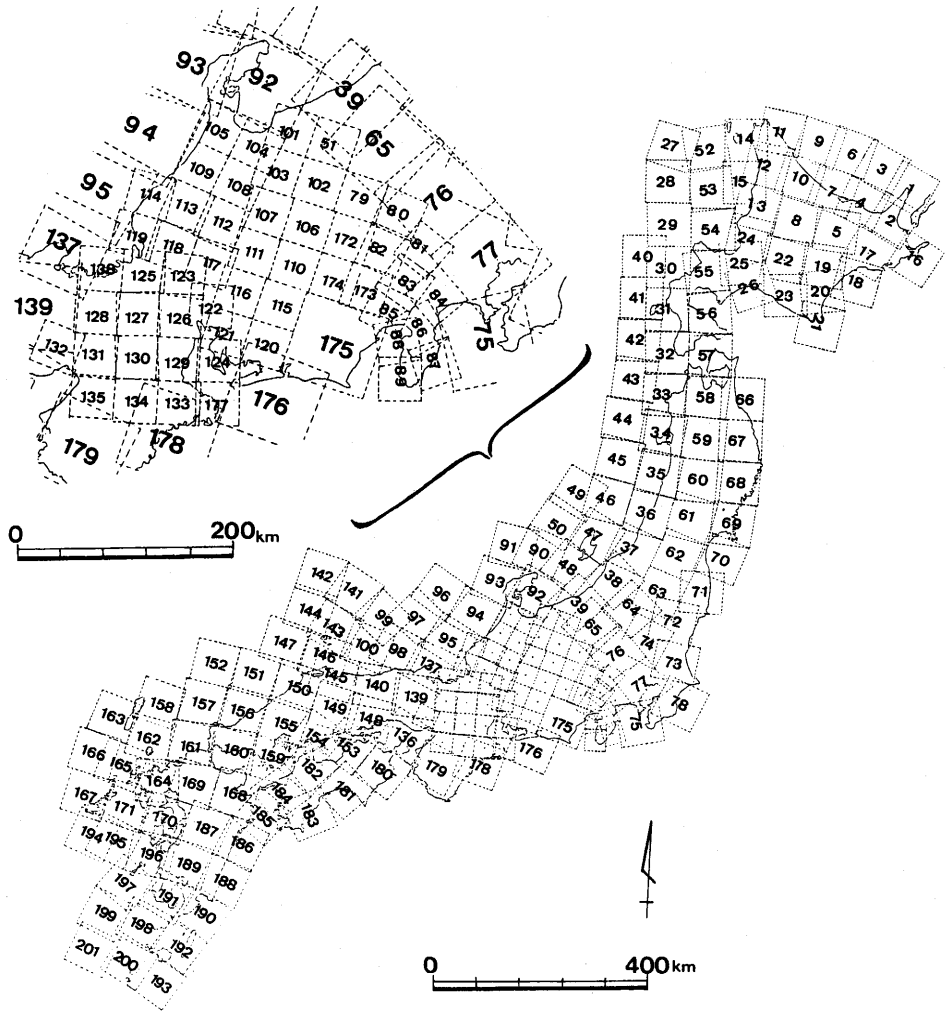

Fig. 4 Grids and grid numbers for calculating strain. The angle of the numeral of each grid represents the direction of maximum shortening. Sizes of the large and small grids are 80 x 80 km^2 and 40 x 40 km^2, respectively.

ferred to the number of the normalized A class thrust fault (N_A^-) which dips at an angle of 45 degrees and strikes perpendicular to the upper side of the grid concerned, and the number of the normalized A class normal fault (N_A^+) which dips at an angle of 45 degrees and strikes parallel to the upper side of the grid concerned, under the assumption that every strike-slip fault has a vertical fault plane; the angle between the strike of fault and the upper or lower side of the grid concerned is 45 degrees, although real angles are varied within 45±15 degrees. From that number (N_A), rates of shortening (R^-) and extension (R^+) were calculated, and then strain rates of shortening (ϵ^-) and extension (ϵ^+) were obtained.

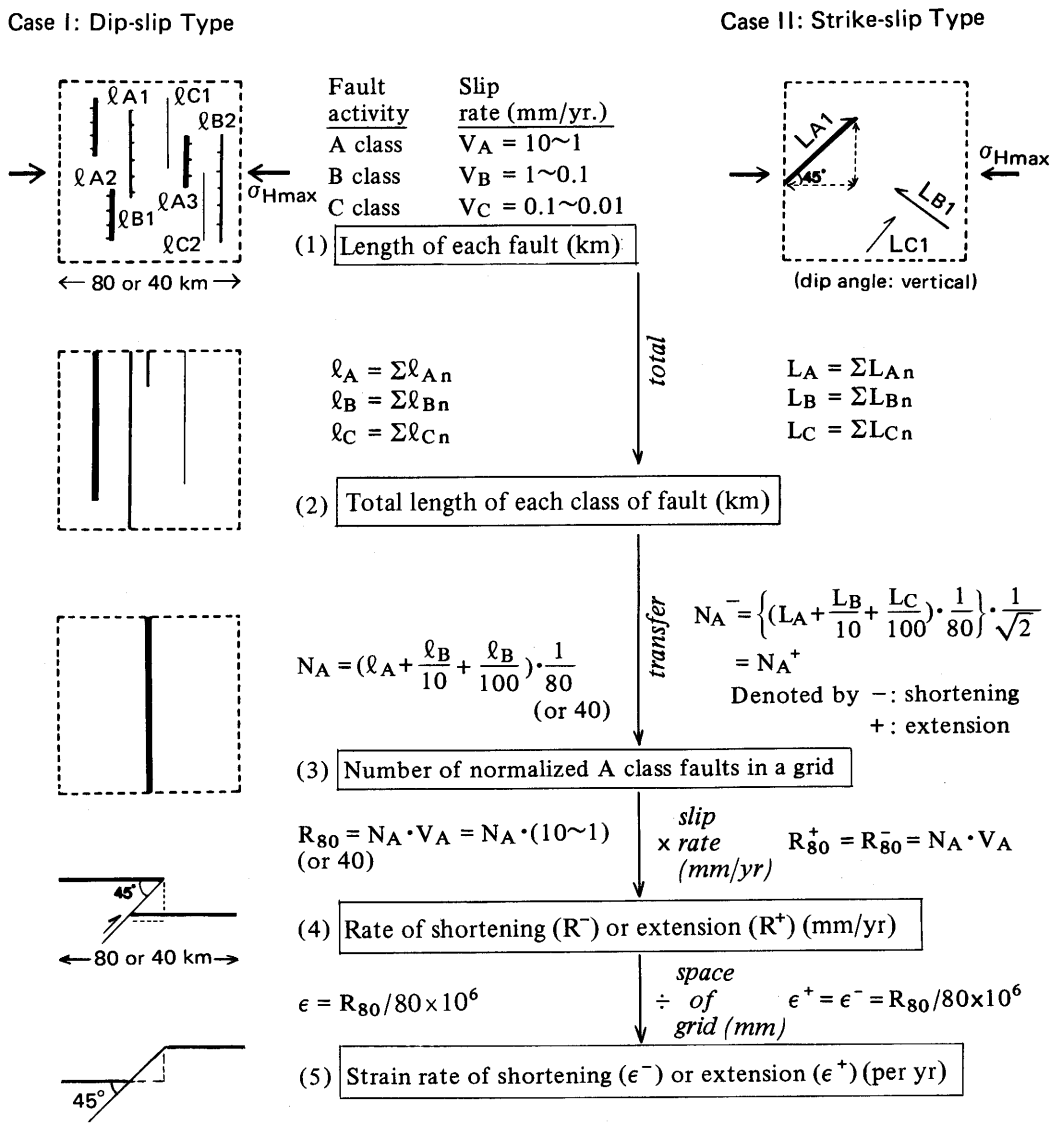

Fig. 5 Procedure of the calculation of strain rates.

Table 2 Length of each class fault and strain rate in every grid.

Province in Fig. 3	Grid no. in Fig. 4	Total length of each class of fault (km) (Fig. 5-(2))								N_A (Fig. 5-(3))		Strain rate ($\times 10^{-6}$/yr.) (Fig. 5-(5))	
		Dip-slip fault†				Strike-slip fault				Dip-slip fault†	Strike-slip fault	Extension ϵ^+	Shortening ϵ^-
		ℓ_A	ℓ_B	(unknown)	ℓ_C	L_A	L_B	(unknown)	L_C				
	1	3		(6)						0.045		*	0.6
	2	33	38							0.460		*	5.8
	3		66		28					0.086		*	1.1
	4	5	92		36					0.162		*	2.0
Ia	5		4		5					0.006		*	0.1
	6		102		100					0.140		*	1.8
	7				20					0.003		*	*
	8		6		7					0.008		*	0.1
	9		24		10					0.031		*	0.4
	10				6					0.001		*	*
	11				9					0.001		*	*
	12				7					0.001		*	*
	13		11							0.014		*	0.2
	14				23					0.003		*	*
Mean value of shortening (ϵ^-) (0.82)	15		8		35					0.014		*	0.2
	16											*	*
	17	5	4							0.068		*	0.9
	18				1.5							*	*
	19		86		30					0.111		*	1.4
	20		83		10					0.105		*	1.3
Ib	21		9		5					0.012		*	0.2
	22		34.5	(20)	4					0.069		*	0.9
	23		4.5	(1)						0.007		*	0.1
	24		2	(8)	19					0.015		*	0.2
	25		19		36					0.028		*	0.4
(0.53)	26		19		37					0.028		*	0.4
	27		134							0.168		*	2.1
	28		158		12					0.199		*	2.5
	29		54		30					0.071		*	0.9
	30		12		70					0.024		*	0.3
	31		18.5	(8)	43					0.039		*	0.5
	32		78		96					0.110		*	1.4
	33		57.5	(4.1)	41.8					0.082		*	1.0
	34		87.9	(16.5)	39					0.135		*	1.7
	35	14	77		93					0.283		*	3.5
	36		22		21					0.030		*	0.4
	37		75		2					0.094		*	1.2
IIa	38	15.5	51.5	(5)	6					0.265		*	3.3
	39	17	205.5	(1)	25					0.473		*	5.9
	40		30		55					0.044		*	0.6
	41				53					0.007		*	0.1
	42		40		26					0.053		*	0.7
	43		30		18					0.040		*	0.5
	44											*	*
	45		104		50					0.136		*	1.7
	46		250		141					0.330		*	4.1
	47		89		109					0.125		*	1.6
	48		110		141					0.155		*	1.9
	49		147		50					0.190		*	2.4
	50		30		20					0.040		*	0.5
(2.46)	(51)	29	68		79					0.920		*	23.0
	52		96		31					0.124		*	1.6
	53		106		68					0.141		*	1.7
IIb	54		81		28					0.105		*	1.3
	55		35	(15)	25					0.066		*	0.8
	56		37.5	(10.5)	2					0.060		*	0.1

Province in Fig. 3	Grid no. in Fig. 4	Total length of each class of fault (km) (Fig. 5-(2))							N_A (Fig. 5-(3))		Strain rate ($\times 10^{-9}$/yr.) (Fig. 5-(5))	
		Dip-slip fault†				Strike-slip fault			Dip-slip fault†	Strike-slip fault	Extension ϵ^+	Shortening ϵ^-
		ℓ_A	ℓ_B	(unknown)	ℓ_C	L_A	L_B	(unknown) L_C				
	57				19				0.002		*	*
	58		67.5		7				0.085		*	*
	59	3	99.5		7				0.163		*	2.0
	60	6	125.5	(36)	9				0.277		*	3.5
IIb	61		76.5	(4)	18				0.103		*	1.3
	62		140		7				0.176		*	2.2
	63		110.5	(26)					0.171		*	2.1
	64		40		15				0.052		*	0.7
(1.70)	65	17	178						0.435		*	5.4
	66		23		2				0.029		*	0.4
	67		36.5						0.046		*	0.6
	68		16						0.020		*	0.3
	69										*	*
III	70		50		3				0.063		*	0.8
	71		76	(6)	10				0.104		*	1.3
	72		46	(29)	5				0.094		*	1.2
	73										*	*
(0.61)	74		51		46				0.070		*	0.9
IVc	75	9	42			22	3		0.165	0.197	2.5	4.5
	76		46		36			15	0.062	0.001	0.1	0.9
	77		41		11	22	4		0.053	0.198	2.5	3.1
	78	21	10				4		0.275	0.004	0.5	3.9
	(79)		5			10.5			0.013	0.186	4.6	5.0
Va	(80)										*	*
	(81)		7		35		11	34	0.026	0.026	0.7	1.3
	(82)	15	18		17				0.424		*	10.6
	(83)	1			11		20		0.028	0.036	0.9	1.6
(5.40)	(84)	29	37		5		32		0.830	0.056	1.4	22.2
	(85)	28	1.5		2		10		0.704	0.018	0.5	18.1
	(86)		6		1.7	13	92.2	7.3	0.015	0.394	9.9	10.2
Vb	(87)				5		10	2	0.001	0.021	0.5	0.6
	(88)	3	6		1.5		31.7	10.8	0.090	0.058	1.5	3.7
(6.74)	(89)				5.5		24	7	0.001	0.044	1.1	1.1
	90		10		54				0.019		*	0.2
	91				38				0.005		*	0.1
VIa	92		162.5		44.5				0.209		*	2.6
	93		20		22				0.028		*	0.4
(1.04)	94			(120)					0.150		*	1.9
	95				110				0.014		*	0.2
	96		43		89				0.065		*	0.8
VIb	97		116		53				0.152		*	1.9
	98		64		24				0.083		*	1.0
	99		35		74				0.053		*	0.7
(0.78)	100		9						0.011		*	0.1
	(101)	15	71		6		10	2	0.554	0.018	0.5	14.3
	(102)	4	78				10		0.295	0.018	0.5	7.8
	(103)		4		15	45		23	0.014	0.800	20.0	20.4
	(104)		13.5		4	40	3	23	0.035	0.716	17.9	18.0
	(105)		89		32				0.231		*	5.8
VIc	(106)	2	84			34	13		0.260	0.624	15.6	22.1
	(107)					10	54	95		0.289	7.2	7.2
	(108)					76	194	62		1.697	42.4	42.4
	(109)		21				20		0.053	0.035	0.9	2.2
	(110)		182	(5)		23	67	(25)	0.468	0.569	14.2	25.9
	(111)				5	82	108	(37)	0.013	1.706	42.7	43.0
	(112)		14.5			2	77	9	0.036	0.173	4.3	5.2

Province in Fig. 3	Grid no. in Fig. 4	Total length of each class of fault (km) (Fig. 5-(2))								N_A (Fig. 5-(3))		Strain rate ($\times 10^{-9}$/yr.) (Fig. 5-(5))	
		Dip-slip fault†				Strike-slip fault				Dip-slip fault†	Strike-slip fault	Extension ϵ^+	Shortening ϵ^-
		ℓ_A	ℓ_B	(unknown)	ℓ_C	L_A	L_B	(unknown)	L_C				
	(113)		27.5				33		9	0.069	0.060	1.5	3.2
	(114)		56.7		1.1		16			0.142	0.028	0.7	4.3
	(115)		64	(8)	3		33	(10)		0.181	0.076	1.9	6.4
	(116)		33				21			0.083	0.037	0.9	3.0
	(117)					25	107.5				0.632	15.8	15.8
	(118)					51	73		7		1.032	25.8	25.8
VIc	(119)		56				15		35	0.140	0.032	0.8	4.3
	(120)								3			*	*
	(121)	16	57		14					0.546		*	13.7
	(122)		74		4					0.186		*	4.7
	(123)		18			47	78.5			0.045	0.970	24.3	25.4
(13.50)	(124)		50		13					0.128		*	3.2
	(125)		73		15		135		9	0.186	0.240	6.0	10.7
	(126)		170.5		19		10			0.431	0.017	0.4	11.2
	(127)		80		37		11			0.209	0.019	0.5	5.7
	(128)		93		19		16		10	0.237	0.030	0.8	6.7
	(129)		82.5		13		22			0.209	0.038	1.0	6.2
VId	(130)		91		95		34		48	0.263	0.069	1.7	8.3
	(131)		146.5		54		21		16	0.380	0.040	1.0	10.5
	(132)		79		20		66		24	0.203	0.121	3.0	8.1
	(133)		11		11				26	0.030	0.005	0.1	0.9
	(134)				4				15	0.001	0.003	0.1	0.1
	(135)		46		39	22	4			0.125	0.396	9.9	13.0
(7.37)	136		71		52.9	7	67.5		22	0.095	1.19	2.7	7.0
	137				57		24		46	0.007	0.025	0.3	0.4
	138						5		20		0.012	0.3	0.3
VIe	139			(15)	66		48	(9)	82	0.003	0.058	0.7	0.8
(0.65)	140				41.8		62	(24)	6	0.005	0.077	1.0	1.1
	141				20					0.003		*	*
	142		59		21					0.076		*	1.0
	143											*	*
	144		80		28					0.104		*	1.3
	145				5.3				19.4	0.001	0.002	*	*
	146				1.8				27.4		0.002	*	*
	147				3							*	*
	148						20	(18)	4		0.034	0.4	0.4
	149						1.5		10		0.002	*	*
	150				7				22.4	0.001	0.002	*	*
	151				10					0.001		*	*
	152				61					0.008		*	0.1
	153		27		4	44	30.2			0.034	0.380	4.8	4.8
VIIa	154			(41)	8		17.5			0.052	0.015	*	0.1
	155		43	(11)	6					0.068		*	0.9
	156											*	*
	157				11							*	*
	158											*	*
	159						43	(27)			0.062	0.8	0.8
	160			(33)			25			0.041	0.022	0.3	0.8
	161		16		5		32	(8)		0.021	0.035	0.4	0.7
	162											*	*
	163				31					0.004		*	0.1
	164				20							*	*
	165				114					0.014		*	0.2
	166			(10)	20					0.015		*	0.2
(0.42)	167				22							*	*

Province in Fig. 3	Grid no. in Fig. 4	Total length of each class of fault (km) (Fig. 5-(2))								N_A (Fig. 5-(3))		Strain rate ($\times 10^{-9}$/yr.) (Fig. 5-(5))	
		Dip-slip fault†				Strike-slip fault				Dip-slip fault†	Strike-slip fault	Extension ϵ^+	Shortening ϵ^-
		ℓ_A	ℓ_B	(unknown)	ℓ_C	L_A	L_B	(unknown)	L_C				
	168	15+	10; 207+		15; 67.8+		28.8			0.014; 0.450+	0.025	6.9	0.8
VIIb	169		83.2+		47.1+		24.7	(8.7)		0.110+	0.030	1.8	0.4
	170		10; 93.1+	(3.5)+						0.013; 0.120+		1.5	0.2
(0.30)	171											*	*
	(172)						36	(21)	17		0.104	2.6	2.6
	(173)	16	7		14					0.421		*	10.5
	(174)		1		14	12	12		47	0.006	0.242	6.0	6.2
	175						20		52		0.024	0.3	0.3
	176								4			*	*
	(177)							(4)			0.010	0.3	0.3
	178								23			*	*
	179		4		8	44			74	0.006	0.395	4.9	5.0
	180					49	21.5	(42)	5.3		0.494	6.2	6.2
	181						10				0.09	0.1	0.1
VIII	182			(8)		66.3	15	(6)	2	0.010	0.605	7.6	7.7
	183			(28.5)						0.036		*	0.5
	184						3.5					*	*
	185			(9)						0.011		*	0.1
	186			(11)						0.014		*	0.2
	187			(4)	1.5		73.9	(115)	4.2	0.005	0.167	2.1	2.7
	188				8							*	*
	189			(22)	8		16			0.029	0.014	0.2	0.4
	190											*	*
	191	10		(22)	8					0.154		*	1.9
	192	1.5			20					0.021		*	0.3
(1.77)	193				36					0.005		*	0.1
	194				58					0.007		*	0.1
	195				28					0.004		*	0.1
	196		56		25		24			0.073	0.021	0.3	1.2
	197		90		52					0.119		*	1.5
X	198	1.5			106					0.032		*	0.4
	199		70		42					0.093		*	1.2
	200		5		82					0.017		*	0.2
(0.69)	201		44		42					0.060		*	0.8

† with out +: thrust fault
with + : normal fault

* less than 0.1

Hybrid cases of dip-slip and strike-slip

When one fault showed both dip-slip and strike-slip components, it was regarded a pure dip-slip or a pure strike-slip fault, on the basis of the larger component of displacement.

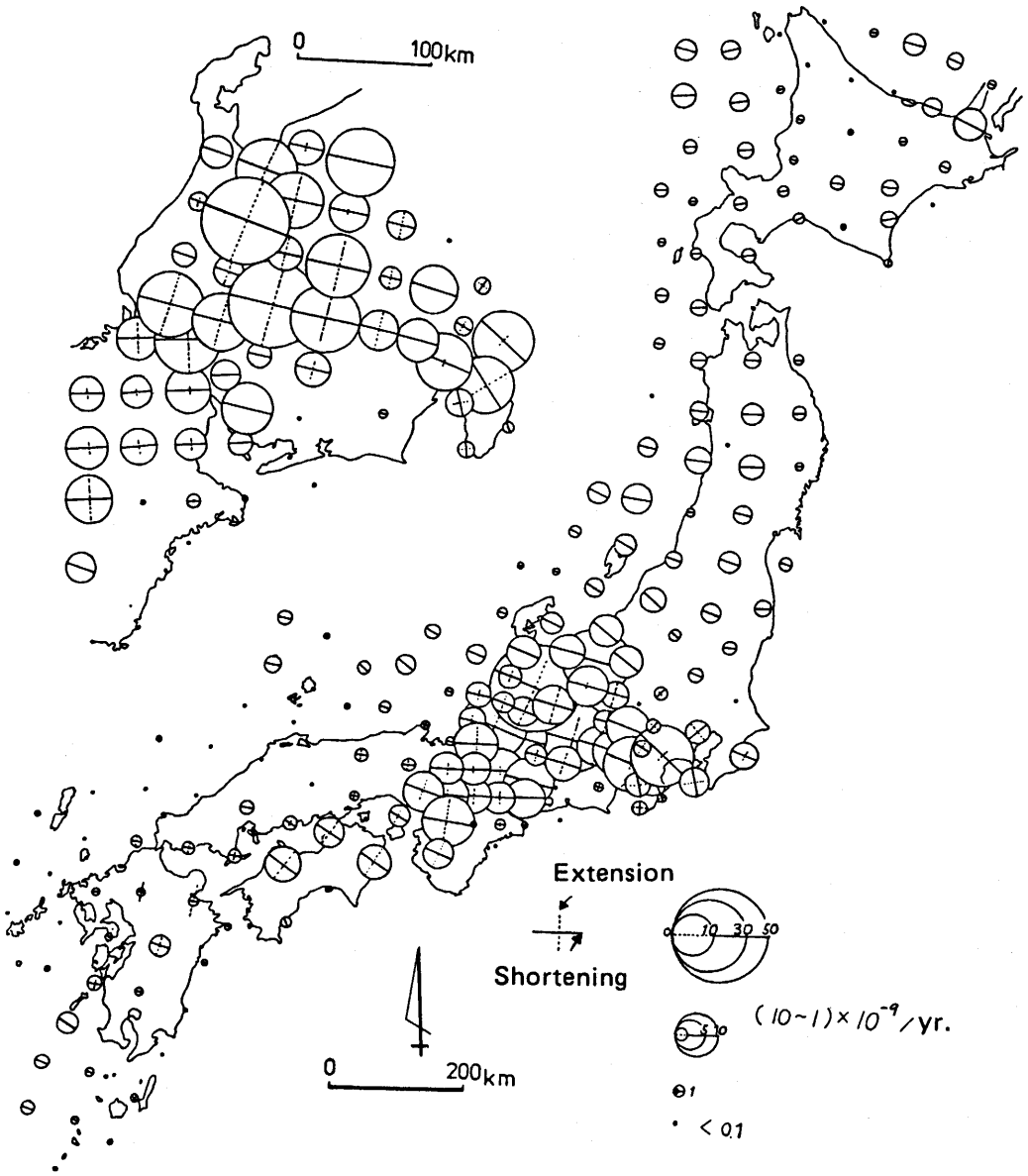

Fig. 6 Strain rates of shortening and extension estimated from the active fault data.
Solid lines show the direction of maximum shortening and its strain rate. Broken lines show the direction of maximum extension and its strain rate. The area of each circle is in proportion to the magnitude of its strain rate of shortening.

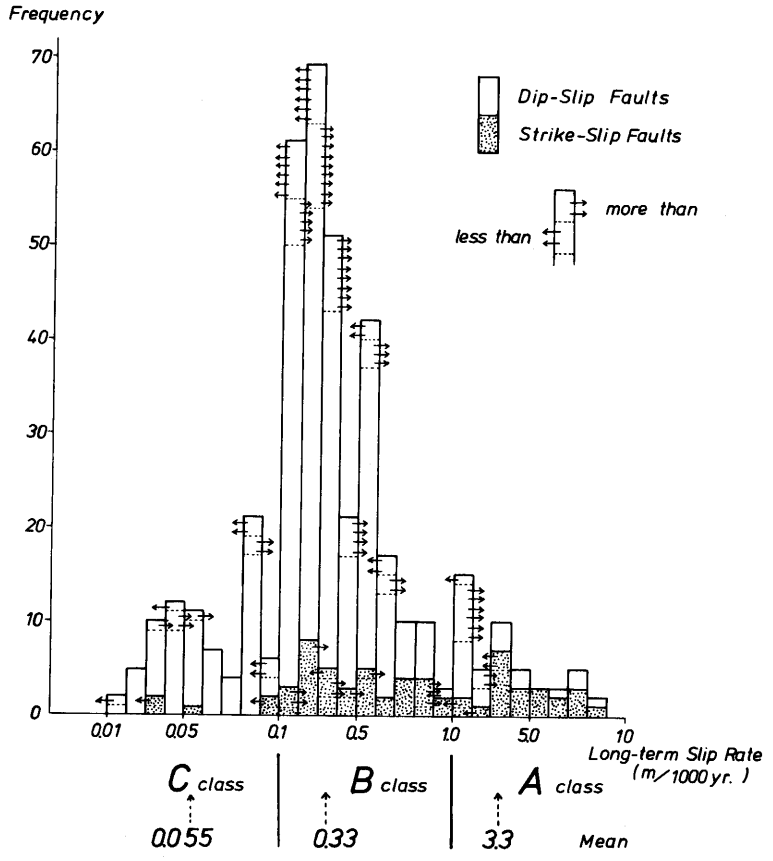

Fig. 7 Frequency distribution of the value-known slip rates of active faults (from the data of RGAF, 1980a).

When both dip-slip and strike-slip faults were mixed in a grid, N_A values and strain rates of shortening and extension were claculated, and, finally, sums of strain rates of shortening (ϵ^-) and extension (ϵ^+) were obtained as shown in Table 2.

Then, based on these data in Table 2, Figure 6 was drawn.

Frequency distribution of slip rates and its use

According to the data in the book of active faults (RGAF, 1980a), values of average slip rates are known for about 20 percent of the total active faults. Based on these known rates, we made a graph of the frequency distribution of slip rates of active faults (Fig. 7), and calculated the mean values of slip rates for each class of fault as shown in Figure 7. From these mean values, it can be said that 3 mm/yr can be used as the value of slip rate for the normalized A class fault (V_A in Fig. 5-(4)) instead of (10~1) mm/yr, as a rough approximation. Accordingly, the unit value of (10~1) x 10^{-9} for the strain rates in Figure 6 can be replaced by 3 x 10^{-9}. In this way – that is, in practice, by multiplying the values of ϵ^- and ϵ^+ (in Table 2) by 3 – distribution maps of strain rates of shortening and extension were obtained (Fig. 8).

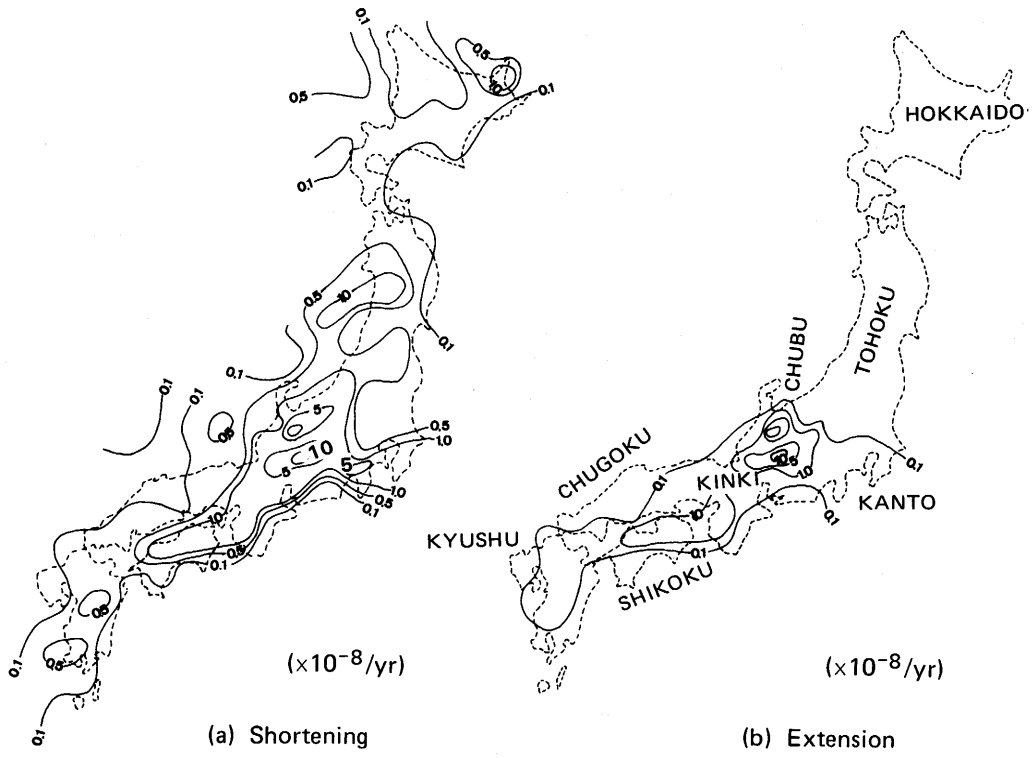

Fig. 8 Distribution of horizontal strain rates of shortening and extension deduced from the active fault data. Instead of (10~1) in Fig. 6, 3 is used for calculation.

3. Results Obtained by the Calculation

Distribution of horizontal strain rates of shortening

Strain rates of shortening in central Japan are greater than those of the other regions (Figs. 6 and 8(a)). In the region connecting southern Kanto – Chubu – Kinki – northern Shikoku (see Fig. 8(b)) for names of districts), the magnitude of the strain rates is from 10^{-7} to 10^{-8}/yr. It is especially great in central Chubu. In northern Kanto, Tohoku, central to southern Kyushu, and northern Hokkaido, it is from 10^{-8} to 10^{-9}/yr, while in the remaining regions it is 10^{-9}/yr and smaller.

Distribution of horizontal strain rates of extension

In the zone connecting southern Kanto – Chubu – Kinki – Shikoku – central Kyushu, the magnitude of strain rates of extension is 10^{-8} to 10^{-9}/yr (Figs. 6 and 8(b)). The region having the greatest magnitude of extension, 10^{-7} to 10^{-8}/yr, is found in the central Chubu mountains, where conjugate sets of NE-SW-trending right lateral and NW-SE-trending left lateral strike-slip faults are closely distributed (Fig. 1). In southern Shikoku, southern Kyushu, and Chugoku, the values of strain rates of extension are as small as 10^{-9}/yr. In central Kyushu, strain rates of extension are greater than those of shortening (Fig. 6), but the magnitude of the former is as small as 10^{-9}/yr. Normal faults in this area are short,

and the degrees of fault activity are not high. In Tohoku and Hokkaido, the magnitude of strain rates of extension is very small or nil, because of very low density or absence of both normal and strike-slip faults.

Distribution of average rates of shortening

Figure 9(a) shows average rates of shortening along the eight bars, which indicate the general directions of maximum shortening and also indicate the length (about 300 km except for the bar in Kanto) from which the average rates of shortening are yielded by compressions. The average rates were calculated generally from the data in four grids (in the case of large grids) along the bars. From this figure, the average rates of shortening are as follows: in central Honshu and southern Kanto, the rate is more than 5 mm/yr, but in other regions, it is around 1 mm/yr.

Figure 9(b) shows the regional average of horizontal strain rates of shortening in each active fault province. In provinces IV, V and VI in central Japan, the strain rates are as large as $1 - 2 \times 10^{-8}$/yr; in the province II, the value is 7×10^{-9}/yr. In other provinces, the values are smaller than 5×10^{-9}/yr.

4. Comparison and Discussion

Our results shown in Figures 6, 8, and 9 are compared with other figures on the strain and strain rate in Japan obtained by various methods, and some related discussions are given below.

Figures 10(a) and (b) are the results obtained by Wesnousky *et al.* (1982) from the data on shallow large earthquakes occurred during the last 400 years and from the data of Quaternary active faults (RGAF, 1980a), respectively. In both cases, the rates of compressive strain and crustal shortening are calculated by use of Kostrov's (1974) formula, relating seismic moment to strain, based upon the seismic moments of 400 years, earthquakes and the expected seismic moments by the Quaternary active faults.

From the comparison between Figures 9 and 10(b), it can be said that the figures on the shortening and the strain rate are nearly the same, if the difference in the way of calculation and the basic data is taken into consideration. Part of the reason that the average rate of shortening in Figure 9(a) is slightly larger than that in Figure 10(b) is due to the difference in the length of base lines and the difference depending on whether submarine active faults are counted in or not.

Figure 11 shows the directions of horizontal maximum shortening and the rates of maximum shear strain which were deduced by Sato (1973) from the changes in horizontal angles between the first (in 1882–1909) and second (in 1948–1967) triangulations. Nearly the same result was obtained by Nakane (1973). The directions of maximum compression are in good harmony with those deduced from active faults shown in Figure 2(a).

When we compare Figure 11 with Figure 8(a), taking the understanding that the value of maximum compressional strain corresponds to 2/3 – 3/4 of the maximum shear strain (Sato, H., personal communication) into consideration, the following may be said. In central Honshu, strain rates are greater than those in the other regions of Japan in both cases, but

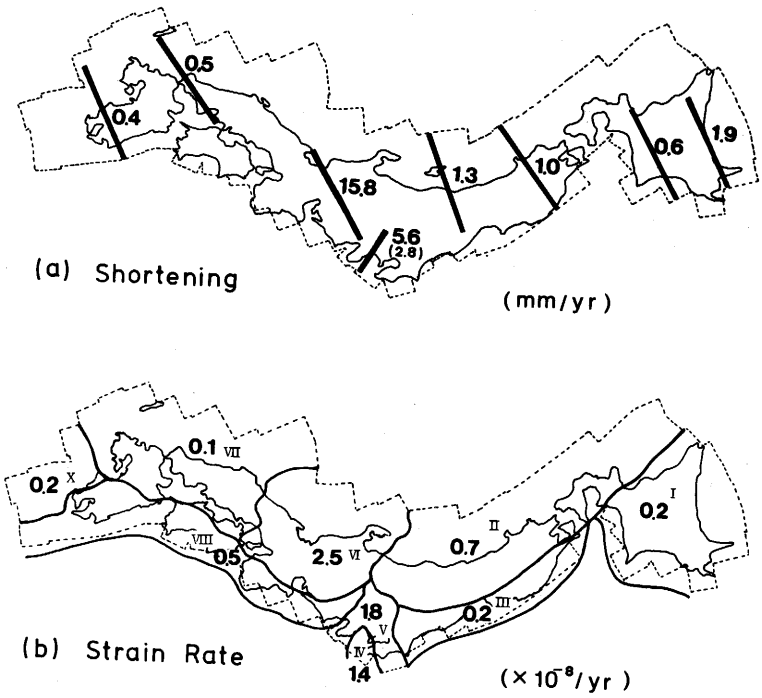

Fig. 9 (a) Average rate of shortening along the bar, showing the maximum shortening direction and the length to be shortened (about 300 km except in the Kanto area, where the rate value 2.8 is for the length to 150 km, and 5.6 for 300 km).
(b) Regional average of horizontal strain rate of shortening in each active fault province (cf. Fig. 3).

the magnitude of strain rate is a little greater in the case of triangulations than in the case of active faults. For northern Honshu, Hokkaido, and Kyushu, the magnitude from the triangulations is mainly $1 - 2 \times 10^{-7}$/yr, while that from the active faults is as small as 10^{-8} to 10^{-9}/yr; thus the difference is quite evident, especially in northewrn Hokkaido and in Kyushu.

As is shown in Figure 10, in northern Honshu, average strain rate deduced from historical earthquakes is about 10 times as great as that from active faults. Wesnousky *et al.* (1982) gave the following explanations for this discrepancy: (1) Northeast Japan is largely overlain by Neogene and Pleistocene sediments, and many faults may possibly remain unrecognized because they do not completely break through the sedimentary cover; (2) offshore earthquakes, having caused a major amount of the moment release and crustal shortening in northern Honshu, were taken into consideration in counting the strain rate, while offshore active faults were not taken into consideration.

The average strain rate deduced from historical earthquakes in northern Honshu is much smaller than the strain rate deduced from triangulations, as is shown in Figure 11. Wesnousky *et al.* (1982) noted that because they measured only the permanent component

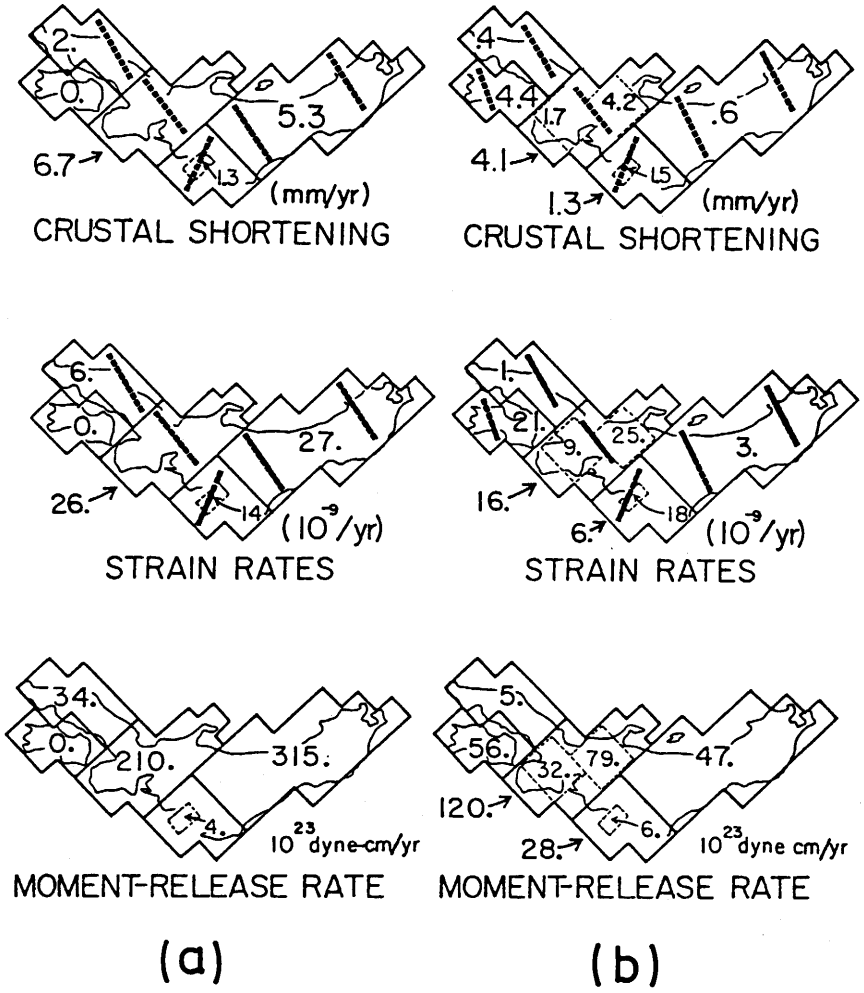

Fig. 10 Regional averages of the rates of moment release, horizontal compressive strain and crustal shortening calculated from the 400-year record of seismicity (a), and those calculated from slip rates of active faults on land using 5, 0.5, and 0.05 mm/yr as slip rates of A, B, and C class faults, respectively. Principal directions of horizontal compressive strain and shortening are denoted by dashed bars (after Wesnousky et al., 1982).

of deformation as accommodated by slip on intraplate faults (just like our measurement of strain), the difference must be attributed to other strain processes. They also wrote that (i) folding may account for part of the difference, and (ii) elastic compressive strain accumulated during the interseismic periods of great interplate earthquakes may also in large part produce the difference.

Quaternary active folds of N-S-trending axes are distributed in the western half of northern Honshu along with N-S-trending active faults. This fold zone has been called the Uetsu fold zone. From Figure 12, in which the rates of strain caused by Quaternary foldings

are shown, it is evident that as far as the western half of northern Honshu is concerned, the strain rate of shortening caused by the Quaternary foldings attains levels of 10^{-6}/yr in places, much greater than the strain rate of shortening caused by the Quaternary faults. It should be noted, however, that the folds having strain rates greater than 10^{-7}/yr generally have wavelengths less than 5 km (Kaizuka, 1968). From such rates of Quaternary folds and the mode of the vertical crustal movements that make mountain ranges, which will be mentioned later, the not-fault-related permanent strain (mainly non-elastic strain) seems to be important in producing the difference between strain rates in northern Honshu (as is shown in Figs. 9 and 11), granting that the elastic compressive strain accumulation during the interseismic period may reach some significant amount (above-mentioned (ii)).

In Hokkaido and Kyushu, there is the same problem as in northern Honshu: that is, what kind of strain process is the principal cause of the great difference between the strain rates deduced from triangulations and those from active faults. Non-elastic strain accumulation in the crust may be worth evaluating concerning this problem.

Itô and Huzita (1974) and Itô *et al.* (1976) treated the problem of mountain-building and shortening of the crust under compressional stresses on the basis of (a) the tectonic history of northern Kinki district in central Honshu and (b) the result of a long-term experiment on the flow of granite under small stresses. In their treatment, the foundation folding, which

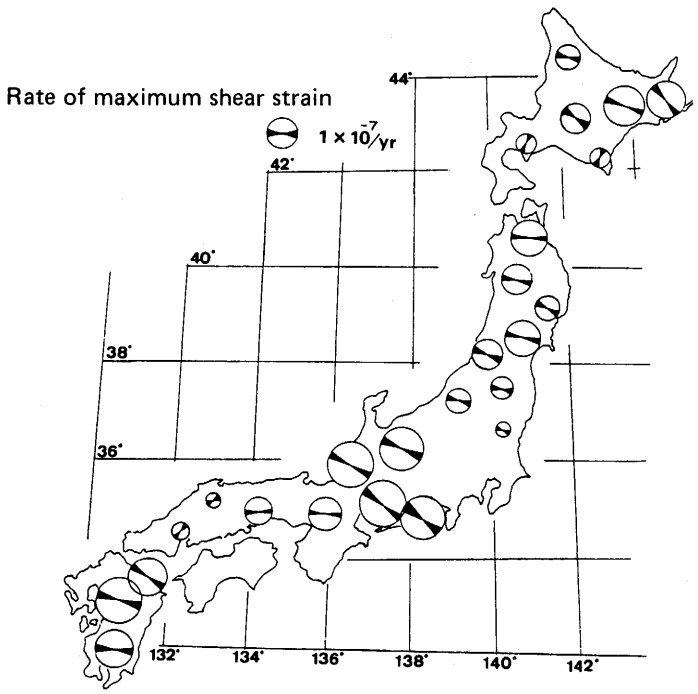

Fig. 11 Strain field of Japan deduced from the changes in horizontal angles of the first-order triangulation during the past ca. 60 years. Narrow fans indicate the direction of maximum shortening and the magnitude of the rate of maximum shear strain (after H. Sato, 1973).

produced 500 m-high ranges and 500 m-deep basins during the past one million years under the condition of isostasy, was explained by non-elastic deformation of the crust; vertical thickening and horizontal shortening in the direction of horizontal compressional stress. In this case, the horizontal strain rate of shortening is counted as large as 5×10^{-15}/sec ($\approx 1.6 \times 10^{-7}$/yr) (cf. Itô, 1979).

The tectonic history of mountain-building in the Uetsu fold zone of northern Honshu is simiar to that in northern Kinki district at least in the Quaternary period, although the Neogene tectonic history of the two regions was quite different. In the Uetsu fold zone, the uplift of mountain ranges during the Quaternary reached around 500 m (Research Group for Quaternary Tectonic Map, 1973). Some of the mountain ranges in the fold zone have active thrust faults of B class on both sides. Therefore, if it is assumed that the vertical slip velocity of a B class fault is 0.3 mm/yr, the mountain growth during the Quaternary attains about 500 m. But in reality, such mountain ranges are rather few, and many have no thrust faults at the foot. Such features suggest that the foundation fold accompanied by few faults is the predominant mode of mountain-building in the Uetsu fold zone.

5. Conclusion

The following are the results obtained from our calculation on the average horizontal strains and strain rates in Japanese main islands and the continental borderlands off the Japan Sea coast from active Quaternary fault data, and from comparing our figures with others obtained so far from other data and by other methods.

1) Average rates of shortening are more than 5 mm/yr in central Honshu and southern Kanto, and around 1 mm/yr in other regions for about 300 km in the directions of maximum shortening.

2) Strain rates of shortening are of the order of 10^{-8}/yr in central Honshu, and of the order of 10^{-9}/yr in other regions on the whole.

3) Strain rates of extension are of the order of 10^{-8}/yr in the central Chubu district and 10^{-9}/yr or less in other regions.

4) Average rates of shortening and strain rates of shortening deduced from active fault data are generally in harmony with those obtained from large shallow earthquakes over the past 400 years.

5) The strain rates of shortening deduced from the changes in horizontal angles of triangulation during the past about 60 years (mainly $1 - 2 \times 10^{-7}$/yr) are much greater than the figures we obtained, especially in Hokkaido and Kyushu.

6) The strain rates of shortening by active Quaternary folding in the western part of northern Honshu, where the wavelengths are smaller than 5 km, are as great as $10^{-7} - 10^{-6}$/yr.

7) The strain rates of crustal shortening by foundation folding in Quaternary Japan seem to be as great as 1×10^{-7}/yr, in Kinki and Tohoku districts at least.

8) The fact that the strain rates of shortening in our calculation are much smaller than those from triangulation data suggests that the not-fault-related permanent strain (mainly non-elastic strain) is important in producing the difference, granting that the elastic com-

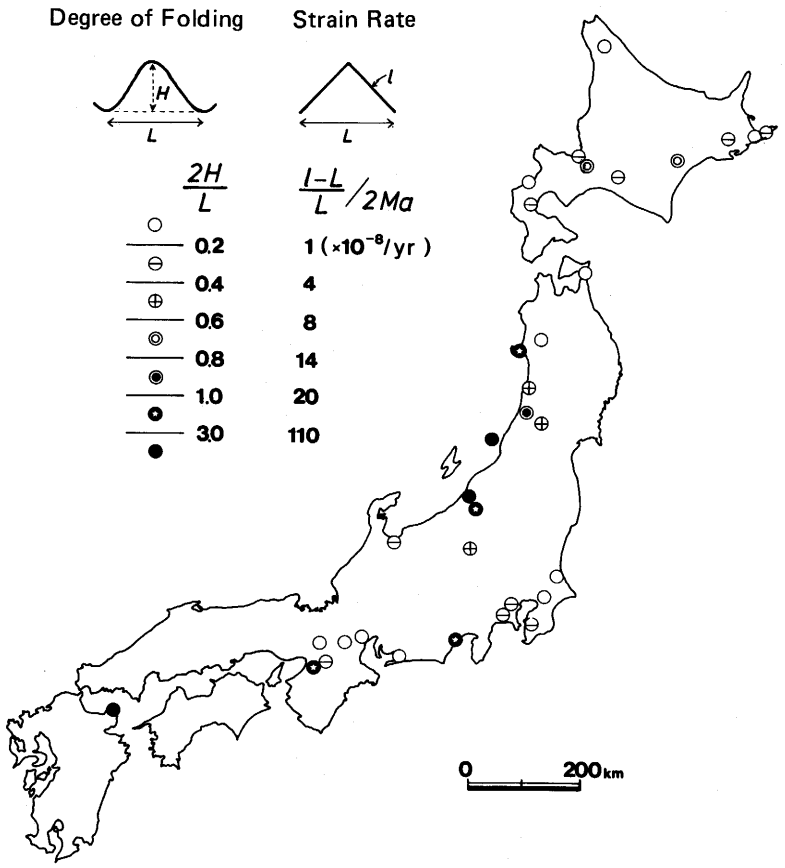

Fig. 12 Distribution of the degrees of Quaternary active foldings and the horizontal strain rates caused by them (after Kaizuka and Murata, 1969). The values of degree of folding are transfered to the horizontal strain rates based on the simple asumption shown in the figure.

pressive strains that have been accumulated during the interseismic periods of great interplate earthquakes may produce a part of the difference; for the process of non-elastic shortening of the upper crust, foundation folding or folding in general seems to be of importance.

Acknowledgements

We thank Professor H. Sato for his information and suggestions on the difference between his results on strain rates deduced from triangulation data and our results. We also thank Ms. M. Uyeda for calculation during the course of this study.

We wish to dedicate this paper to Professor Takamasa Nakano in commemoration of his retirement from Tokyo Metropolitan University.

References Cited

Itô, H. (1979): Rheology of the crust based on long-term creep tests of rocks. *Tectonophysics,* **52,** 629–641.

— and Huzita, K. (1974): The flow of the earth's crust considered from Quaternary crustal movements in Southwest Japan. Rock Mech. in Japan, **2,** 181–183.

—, Oka, Y. and Huzita, K. (1976): The shortening Japanese Islands*. *Kagaku (Science),* **46,** 745–754.

Kaizuka, S. (1968): Distribution of Quaternary folds, especially rate and axis direction in Japan. *Geogr. Rep. Tokyo Metropol. Univ.* **3,** 1–9.

— and Imaizumi, T. (1981): Horizontal strain rates of the Japanese Islands estimated from active fault data.* *Programme & Abst. Seismol. Soc. Japan, 1981,* No. 1, 54.

—, and Murata, A. (1969): The amounts of crustal movements during the Neogene and the Quaternary in Japan. *Geogr. Rep. Tokyo Metropol.* Univ. **4,** 1–10.

Kakimi, T. (1983): Regional interrelation between active faults and destructive earthquakes on land in Japan.** *Bull. Geol. Surv. Japan,* **34,** 295–309.

Kostrov, B.V. (1974): Seismic moment and energy of earthquakes, and seismic flow of rocks. *Izv. Acad. Sci. USSR Phys. Solid Earth,* **1,** 23–40.

Matsuda, T. (1981): Active faults and damaging earthquakes in Japan – macroscopic zoning and precaution fault zones, in Simpson, D.W. and Richards, P.G. (eds.): *Earthquake Prediction; an international review.* Am. Geophy. Union, 279–289.

—, Nakamura, K., and Sugimura, A. (1978): Active faults and Neotectonics, in Kasahara, K. and Sugimura, A. (eds.): *Iwanami Koza Chikyukagaku (Earth Science Series),* **10,** Iwanami Shoten, Tokyo, 89–157.

Nakane, K. (1973): Horizontal tectonic strain in Japan (I) (II).** *Jour. Geodetic Soc. Japan,* **19,** 190–199, 200–208.

Research Group for Active Faults (1980a): Active faults in Japan: sheet maps and inventories.** Univ. of Tokyo Press, 363p.

Research Group for Active Faults of Japan (1980b): Active Faults in and around Japan: the distribution and the degree of activity. *Jour. National Disaster Sci.,* **2,** 61–99.

Research Group for Quaternary Tectonic Map (1973): Explanatory text of the Quaternary Tectonic Map of Japan. Natl. Res. Cent. for Disaster Prevention, Sci. and Tech. Agency, Tokyo, 167p.

Sato, H. (1973): A study of horizontal movement of the earth crust associated with destructive earthquakes in Japan. *Bull. Geogr. Surv. Inst.* **19,** 89–130.

Usami, T. (1975): *Descriptive Catalogue of Disaster Earthquakes in Japan.** Univ. Tokyo Press, Tokyo, 327 p.

Wesnousky, S.G., Scholz, G.H. and Shimazaki, K. (1982): Deformation of an island arc: rates of moment release and crustal shortening in intraplate Japan determined from seismicity and Quaternary fault data. *Jour. Geophy. Res.* **87,** B8, 6829–6852.

(* in Japanese, ** in Japanese with English abstract)